

# Microscopic calculation of ${}^6\text{Li}$ elastic and transition form factors

R.B. Wiringa

*Physics Division, Argonne National Laboratory, Argonne, Illinois 60439*

R. Schiavilla

*Jefferson Lab, Newport News, Virginia 23606*

*and*

*Department of Physics, Old Dominion University, Norfolk, Virginia 23529*

(December 2, 2024)

## Abstract

Variational Monte Carlo wave functions, obtained from a realistic Hamiltonian consisting of the Argonne  $v_{18}$  two-nucleon and Urbana-IX three-nucleon interactions, are used to calculate the  ${}^6\text{Li}$  ground-state longitudinal and transverse form factors as well as transition form factors to the first four excited states. The charge and current operators include one- and two-body components, leading terms of which are constructed consistently with the two-nucleon interaction. The calculated form factors and radiative widths are in good agreement with available experimental data.

PACS numbers: 21.45.+v,25.30.Bf,25.30.Dh,27.20.+n

arXiv:nucl-th/9807037v1 10 Jul 1998

Calculations of the  ${}^6\text{Li}$  elastic and inelastic form factors have relied in the past on relatively simple shell-model [1–3] or  $\alpha$ - $d$  [4] cluster wave functions. These calculations have typically failed to provide a satisfactory, quantitative description of all measured form factors. More phenomenologically successful models have been based on  $\alpha NN$  [5–8] clusterization, or on extensions of the basic spherical-cluster  $\alpha$ - $d$  model in which the deuteron is allowed to deform [9]. However, while these models do provide useful insights into the structure of the  $A=6$  nuclei, their connection with the underlying two- (and three-) nucleon dynamics is rather tenuous.

The  ${}^6\text{Li}$  form factor calculations we report on here are within the context of a realistic approach to nuclear dynamics based on two- and three-nucleon interactions—the Argonne  $v_{18}$  [10] and Urbana IX [11] interactions, respectively, or AV18/UIX model—and consistent two-body charge and current operators [12–14]. Up until very recently, calculations of this type were limited to the  $A=2$ –4 systems, as reviewed in Ref. [15]. Indeed, the deuteron structure functions and threshold electrodisintegration, the trinucleon charge and magnetic form factors, and  $\alpha$  charge form factor have been the observables of choice for testing the quality of interactions and associated two-body currents. However, the availability of realistic six-body wave functions for the ground and low-lying excited states of  ${}^6\text{Li}$  [16] makes it now possible to extend and test our understanding of the electromagnetic structure of nuclei in a new regime—that of p-shell nuclei—and to verify to what extent the inability of reproducing simultaneously the observed elastic and transition form factors is due to the inadequacy of cluster or shell-model wave functions.

The AV18/UIX model reproduces the experimental binding energies and charge radii of  ${}^3\text{H}$ ,  ${}^3\text{He}$ , and  ${}^4\text{He}$  in numerically exact calculations, based on the Faddeev [17], pair-correlated hyperspherical harmonics [18], and Green’s function Monte Carlo (GFMC) [16] methods. For  $A=6$  systems the GFMC results are somewhat underbound compared to the experimental ground states, by 2% in  ${}^6\text{Li}$  and 5% in  ${}^6\text{He}$  and  ${}^6\text{Be}$ . The best variational Monte Carlo (VMC) energies are an additional 10% above the GFMC results. However, the known excitation spectra are well reproduced by both VMC and GFMC calculations. These include, in order of excitation, the states with spin, parity, and isospin assignments,  $(J^\pi; T)$ , of  $(3^+; 0)$ ,  $(0^+; 1)$ ,  $(2^+; 0)$ , and  $(2^+; 1)$  [16].

The variational wave function for  $A=6$  nuclei used here is the trial wave function,  $\Psi_T$ , that serves as the starting point for the GFMC calculations. It has the general form

$$|\Psi_T\rangle = \left[ 1 + \sum_{i<j<k} \tilde{U}_{ijk}^{TNI} \right] \left[ \mathcal{S} \prod_{i<j} (1 + U_{ij}) \right] |\Psi_J\rangle, \quad (1)$$

where  $U_{ij}$  and  $\tilde{U}_{ijk}^{TNI}$  are two- and three-body correlation operators and the Jastrow wave function  $|\Psi_J\rangle$  is given by

$$|\Psi_J\rangle = \mathcal{A} \left\{ \prod_{i<j<k\leq 4} f_{ijk}^c \prod_{i<j\leq 4} f_{ss}(r_{ij}) \prod_{k\leq 4} f_{sp}(r_{k5}) f_{sp}(r_{k6}) \sum_{LS} \left( \beta_{LS} f_{pp}^{LS}(r_{56}) |\Phi_6(LSJM T T_3)_{1234:56}\rangle \right) \right\}. \quad (2)$$

The  $\mathcal{S}$  and  $\mathcal{A}$  are symmetrization and antisymmetrization operators, respectively. The central pair and triplet correlations  $f_{xy}(r_{ij})$  and  $f_{ijk}^c$  are functions of relative position only;

the subscripts  $xy$  denote whether the particles are in the s- or p-shell. The  $|\Phi_6(LSJMTT_3)\rangle$  is a single-particle wave function with orbital angular momentum  $L$  and spin  $S$  coupled to total angular momentum  $J$ , projection  $M$ , isospin  $T$ , and charge state  $T_3$ :

$$\begin{aligned} |\Phi_6(LSJMTT_3)_{1234;56}\rangle &= |\Phi_4(0000)_{1234}\phi_p^{LS}(R_{\alpha 5})\phi_p^{LS}(R_{\alpha 6}) \\ &\left\{ [Y_{1m_l}(\Omega_{\alpha 5})Y_{1m'_l}(\Omega_{\alpha 6})]_{LM_L} \times [\chi_5(\tfrac{1}{2}m_s)\chi_6(\tfrac{1}{2}m'_s)]_{SM_S} \right\}_{JM} \\ &\times [\nu_5(\tfrac{1}{2}t_3)\nu_6(\tfrac{1}{2}t'_3)]_{TT_3} . \end{aligned} \quad (3)$$

Particles 1–4 are placed in an  $\alpha$  core with only spin-isospin degrees of freedom, denoted by  $\Phi_4(0000)$ , while particles 5–6 are placed in  $p$ -wave orbitals  $\phi_p^{LS}(R_{\alpha k})$  that are functions of the distance between the center of mass of the  $\alpha$  core and particle  $k$ . Different amplitudes  $\beta_{LS}$  are mixed to obtain an optimal wave function; for the  $(1^+; 0)$  ground state of  ${}^6\text{Li}$  we mix  $\beta_{01}$ ,  $\beta_{10}$ , and  $\beta_{21}$  terms, while both the  $(3^+; 0)$  and  $(2^+; 0)$  states are “stretch” states and use only  $\beta_{21}$ . For the  $(0^+; 1)$  excited state the  $\beta_{00}$  and  $\beta_{11}$  amplitudes contribute, and for  $(2^+; 1)$  the wave function is constructed from  $\beta_{20}$  and  $\beta_{11}$  terms.

The two-body correlation operator  $U_{ij}$  is defined as:

$$U_{ij} = \sum_{p=2,6} \left[ \prod_{k \neq i,j} f_{ijk}^p(\mathbf{r}_{ik}, \mathbf{r}_{jk}) \right] u_p(r_{ij}) O_{ij}^p , \quad (4)$$

where the  $O_{ij}^{p=2,6} = \boldsymbol{\tau}_i \cdot \boldsymbol{\tau}_j$ ,  $\boldsymbol{\sigma}_i \cdot \boldsymbol{\sigma}_j$ ,  $\boldsymbol{\sigma}_i \cdot \boldsymbol{\sigma}_j \boldsymbol{\tau}_i \cdot \boldsymbol{\tau}_j$ ,  $S_{ij}$ , and  $S_{ij} \boldsymbol{\tau}_i \cdot \boldsymbol{\tau}_j$ . The six radial functions  $f_{ss}(r)$  and  $u_{p=2,6}(r)$  are obtained from approximate two-body Euler-Lagrange equations with variational parameters [19]. The  $f_{sp}$  and  $f_{pp}^{LS}$  correlations are similar to  $f_{ss}$  for small separations, but include long-range tails. The parameters used in constructing these two-body correlations, as well as the description of the three-body correlation operator  $\tilde{U}_{ijk}^{TNI}$  and the operator-independent three-body correlations  $f_{ijk}^c$  and  $f_{ijk}^p$  are given in Ref. [16].

Energy expectation values are evaluated using a Metropolis Monte Carlo algorithm [19]. The VMC results for the ground and low-lying excited states of  ${}^6\text{Li}$  are compared to the GFMC and experimental energies [20] in Table I. The ground state is underbound by nearly 5 MeV compared to experiment, and is only 0.1 MeV more bound than the corresponding  ${}^4\text{He}$  calculation (26.9 MeV). This is above the threshold for breakup of  ${}^6\text{Li}$  into an  $\alpha$  and a deuteron; in principle, it should be possible to lower the variational energy at least to that threshold, but the wave function would be greatly spread out. We have chosen to constrain our parameter search to keep the rms point-nucleon radius for the ground state near the experimental value of 2.43 fm. Despite the large energy deficit compared to the GFMC calculation, the VMC and GFMC one-body densities in  ${}^6\text{Li}$  are virtually identical. However, the two-body GFMC densities are somewhat larger near their peak at  $r_{ij} \approx 1$  fm [16].

The nuclear charge and current operators consist of one- and two-body terms. We here summarize their most important features, and refer the reader to Refs. [15,21] for a listing of the explicit expressions. The two-body current operator has “model-independent” and “model-dependent” components, in the classification scheme of Riska [22]. The model-independent terms are obtained from the charge-independent part of the AV18, and by construction [23] satisfy current conservation with this interaction. The leading operator is the isovector “ $\pi$ -like” current obtained from the isospin-dependent spin-spin and tensor

interactions. The latter also generate an isovector “ $\rho$ -like” current, while additional model-independent isoscalar and isovector currents arise from the isospin-independent and isospin-dependent central and momentum-dependent interactions. These currents are short-ranged and numerically far less important than the  $\pi$ -like current.

The model-dependent currents are purely transverse and therefore cannot be directly linked to the underlying two-nucleon interaction. The present calculation includes the isoscalar  $\rho\pi\gamma$  and isovector  $\omega\pi\gamma$  transition currents as well as the isovector current associated with excitation of intermediate  $\Delta$ -isobar resonances. The  $\rho\pi\gamma$  and  $\omega\pi\gamma$  couplings are known from the measured widths of the radiative decays  $\rho \rightarrow \pi\gamma$  [24] and  $\omega \rightarrow \pi\gamma$  [25], respectively, while their momentum-transfer dependence is modeled using vector-meson-dominance. The M1  $\gamma N\Delta$  coupling is obtained from an analysis of  $\gamma N$  data in the  $\Delta$ -resonance region [26]. Monopole form factors are introduced at the meson-baryon vertices with cutoff values of  $\Lambda_\pi=3.8 \text{ fm}^{-1}$  at the  $\pi NN$  and  $\pi N\Delta$  vertices and  $\Lambda_\rho=\Lambda_\omega=6.3 \text{ fm}^{-1}$  at the  $\rho NN$  and  $\omega NN$  vertices.

While the main parts of the two-body currents are linked to the form of the two-nucleon interaction through the continuity equation, the most important two-body charge operators are model-dependent, and should be considered as relativistic corrections. Indeed, a consistent calculation of two-body charge effects in nuclei would require the inclusion of relativistic effects in both the interaction models and nuclear wave functions. Such a program is just at its inception for systems with  $A \geq 3$ . There are nevertheless rather clear indications for the relevance of two-body charge operators from the failure of the impulse approximation (IA) in predicting the charge form factors of the three- and four-nucleon systems [15]. The model commonly used [13,15] includes the  $\pi$ -,  $\rho$ -, and  $\omega$ -meson exchange charge operators with both isoscalar and isovector components, as well as the (isoscalar)  $\rho\pi\gamma$  and (isovector)  $\omega\pi\gamma$  charge transition couplings, in addition to the single-nucleon Darwin-Foldy and spin-orbit relativistic corrections. It should be emphasized, however, that for  $q < 5 \text{ fm}^{-1}$  the contribution due to the  $\pi$ -exchange charge operator is typically an order of magnitude larger than that of any of the remaining two-body mechanisms and one-body relativistic corrections.

We have calculated longitudinal  $F_L(q)$  and transverse  $F_T(q)$  form factors of the  ${}^6\text{Li}$  ground state as well as transitions from this to the first four excited states. The Coulomb (CJ) multipoles contributing to  $F_L(q)$  are obtained from matrix elements of the charge operator,  $\rho(\mathbf{q})$ , while the electric (EJ) and/or magnetic (MJ) multipoles contributing to  $F_T(q)$  are obtained from matrix elements of the current operator,  $\mathbf{j}(\mathbf{q})$ , using standard formulas [27].

Our elastic form factors  $F_L(q)$  and  $F_T(q)$  are compared with the experimental values [9,28–30] in Fig. 1. Since the  ${}^6\text{Li}$  ground state is  $(1^+;0)$ , both C0 and C2 multipoles contribute to  $F_L(q)$ , while only the M1 operator contributes to  $F_T(q)$ . The results obtained in both IA and with inclusion of two-body corrections in the charge and current operators (IA+MEC) are displayed, along with the statistical errors associated with the Monte Carlo integrations. The  $F_L(q)$  is in excellent agreement with experiment; in particular, the two-body contributions (predominantly due to the  $\pi$ -like charge operator) shift the minimum to lower values of  $q$ , consistent with what has been found for the charge form factors of the hydrogen and helium isotopes [15]. The C2 contribution is much smaller than C0 below  $3 \text{ fm}^{-1}$ , as shown in Fig. 1, and at low  $q$  is proportional to the ground state quadrupole moment. Our prediction for the latter is  $-0.23(9) \text{ fm}^2$ , larger (though with a 50% statistical error) in absolute value than the measured value of  $-0.08 \text{ fm}^2$ , but with the correct (nega-

tive) sign. Cluster models of the  ${}^6\text{Li}$  ground state generally give large, positive values for the quadrupole moment, presumably due to the lack of D-waves in the  $\alpha$ , and the consequent absence of destructive interference between these and the D-wave in the  $\alpha$ - $d$  relative motion [8]. For  $q \geq 3 \text{ fm}^{-1}$ , the C2 contribution becomes dominant, and the shoulder seen in the data is entirely due to this component, which has frequently been omitted from cluster models.

The experimental  $F_T(q)$  is well reproduced by our calculations in the first peak at  $q = 0.5 \text{ fm}^{-1}$ , but the zero comes a little too early and the second peak at  $q = 2 \text{ fm}^{-1}$  is somewhat overpredicted. Since the  ${}^6\text{Li}$  ground state has  $T=0$ , only isoscalar two-body currents contribute to  $F_T(q)$ ; the associated contributions are small at low  $q$ , but increase with  $q$ , becoming significant for  $q > 3 \text{ fm}^{-1}$ , beyond the range of present data. The calculated magnetic moment is  $0.829 \mu_N$  in IA and  $0.832 \mu_N$  with two-body currents, about 1% larger than the experimental value, which is close to that of a free deuteron.

The calculated longitudinal inelastic form factor to the  $(3^+;0)$  state is found to be in excellent agreement with experiment [29,31,32], as shown in Fig. 2. This transition is induced by C2 and C4 operators, and thus the associated form factor  $F_L(q)$  behaves as  $q^4$  at low  $q$ . The two-body contributions only become important for  $q > 2 \text{ fm}^{-1}$ , but do improve the agreement with data. We also show our prediction for the much smaller transverse form factor  $F_T(q)$ . The calculated radiative width of the  $(3^+;0)$  state is  $3.38(9) \times 10^{-4} \text{ eV}$  in both IA and with MEC, compared to the experimental value of  $(4.40 \pm 0.34) \times 10^{-4} \text{ eV}$  [33].

Good agreement is also found with the experimental values [3,32] for the transverse inelastic form factor to the state  $(0^+;1)$ , as shown in Fig. 2. This is an isovector magnetic dipole transition and, as expected, is significantly influenced, even at low values of  $q$ , by two-body contributions, predominantly by those due to the  $\pi$ -like current operator. The predicted radiative width is  $7.49(2) \text{ eV}$  in IA and  $9.06(7) \text{ eV}$  including MEC, compared with the experimental value  $8.19 \pm 0.17 \text{ eV}$ . Thus the isovector two-body current contributions increase the  $\gamma$ -width by 20%.

The calculated longitudinal and transverse inelastic form factors to the  $(2^+;0)$  state are also shown in Fig. 2. The contributing multipole operators are C2 for the longitudinal transition, and M1, E2, and M3 for the transverse transition. The  $F_L(q)$  is comparable in magnitude to that for the  $(3^+;0)$  state, but has not been measured to date; the  $F_T(q)$  is again much smaller. The corresponding  $\gamma$ -width is calculated at  $8.0(5) \times 10^{-3} \text{ eV}$  both in IA and with MEC. This result just overlaps the experimental value of  $(5.4 \pm 2.8) \times 10^{-3} \text{ eV}$  [33].

Finally, we show the inelastic form factors to the  $(2^+;1)$  state. For this isovector transition, the  $F_T(q)$  is much larger than the  $F_L(q)$ . The experimental data [4,32,33] are well reproduced by the calculation, with the two-body currents contributing significantly at all  $q$  values. However the calculated  $\gamma$ -width of  $0.050(9) \text{ eV}$  in IA and  $0.075(26) \text{ eV}$  with MEC is several times smaller than the reported experimental value of  $0.27 \pm 0.05 \text{ eV}$ .

To summarize, we have presented the first *ab initio* microscopic calculations of  ${}^6\text{Li}$  elastic and transition form factors, based on six-body VMC wave functions obtained from realistic interactions and a consistent, realistic nuclear electromagnetic current operator. We do not expect that use of the more accurate GFMC wave functions will lead to significantly different predictions, since the VMC and GFMC one- and two-body densities have been found to be quite close [16]. Inclusion of the contributions from two-body charge and current operators brings theory into significantly better agreement with the experimental data. Thus

nuclear many-body theory appears to provide a quantitatively satisfactory description of the electromagnetic structure of both s- and p-shell nuclei for a wide range of momentum transfers. We re-emphasize that reproducing simultaneously all measured form factors of the  ${}^6\text{Li}$  low-lying states had proven, in the past, problematic with both shell-model and cluster-model wave functions.

#### ACKNOWLEDGMENTS

The authors wish to thank J. Carlson, D. Kurath, V.R. Pandharipande, and S.C. Pieper for many useful comments. Computations were performed on the IBM SP of the Mathematics and Computer Science Division, Argonne National Laboratory. The work of RBW is supported by the U. S. Department of Energy, Nuclear Physics Division, under contract No. W-31-109-ENG-38, and that of RS by the U. S. Department of Energy.

## REFERENCES

- [1] T.W. Donnelly and J.D. Walecka, Phys. Lett. B **44**, 330 (1973).
- [2] J.D. Vergados, Nucl. Phys. A **220**, 259 (1974).
- [3] J.C. Bergstrom, I.P. Auer, and R.S. Hicks, Nucl. Phys. A **251**, 401 (1975).
- [4] J.C. Bergstrom, Nucl. Phys. A **327**, 458 (1979).
- [5] D.R. Lehman and W.C. Parke, Phys. Rev. Lett. **50**, 98 (1983).
- [6] D.R. Lehman and W.C. Parke, Phys. Rev. C **28**, 364 (1983).
- [7] V.I. Kukulín, V.T. Voronchev, T.D. Kaipov, and R.A. Eramzhyan, Nucl. Phys. A **517**, 221 (1990).
- [8] V.I. Kukulín, V.N. Pomerantsev, Kh.D. Razikov, V.T. Voronchev, and G.G. Ryzhikh, Nucl. Phys. A **586**, 151 (1995).
- [9] J.C. Bergstrom, S.B. Kowalski, and R. Neuhausen, Phys. Rev. C **25**, 1156 (1982).
- [10] R.B. Wiringa, V.G.J. Stoks, and R. Schiavilla, Phys. Rev. C **51**, 38 (1995).
- [11] B.S. Pudliner, V.R. Pandharipande, J. Carlson, and R.B. Wiringa, Phys. Rev. Lett. **74**, 4396 (1995).
- [12] R. Schiavilla, V.R. Pandharipande, and D.O. Riska, Phys. Rev. C **40**, 2294 (1989).
- [13] R. Schiavilla, V.R. Pandharipande, and D.O. Riska, Phys. Rev. C **41**, 309 (1990).
- [14] J. Carlson, D.O. Riska, R. Schiavilla, and R.B. Wiringa, Phys. Rev. C **42**, 830 (1990).
- [15] J. Carlson and R. Schiavilla, Rev. Mod. Phys. in press (1998).
- [16] B.S. Pudliner, V.R. Pandharipande, J. Carlson, S.C. Pieper, and R.B. Wiringa, Phys. Rev. C **56**, 1720 (1997).
- [17] A. Nogga, D. Hüber, H. Kamada, and W. Glöckle, Phys. Lett. B **409**, 19 (1997).
- [18] A. Kievsky, M. Viviani, and S. Rosati, Phys. Rev. C **52**, R15 (1995).
- [19] R.B. Wiringa, Phys. Rev. C **43**, 1585 (1991).
- [20] F. Ajzenberg-Selove, Nucl. Phys. A **490**, 1 (1988).
- [21] M. Viviani, R. Schiavilla, and A. Kievsky, Phys. Rev. C **54**, 534 (1996).
- [22] D.O. Riska, Phys. Rep. **181**, 207 (1989).
- [23] D.O. Riska, Phys. Scr. **31**, 471 (1985).
- [24] H. Berg *et al.*, Nucl. Phys. A **334**, 21 (1980).
- [25] M. Chemtob and M. Rho, Nucl. Phys. A **163**, 1 (1971); **212**, 628(E).
- [26] C.E. Carlson, Phys. Rev. D **34**, 2704 (1986).
- [27] T. deForest and J.D. Walecka, Adv. Phys. **15**, 1 (1966).
- [28] L. Lapikás, *Proceedings of the Conference on Modern Trends in Elastic Electron Scattering*, edited by C. De Vries (NIKHEF-K, Amsterdam, 1978).
- [29] G.C. Li, I. Sick, R.R. Whitney, and M.R. Yearian, Nucl. Phys. A **162**, 583 (1971).
- [30] R.E. Rand, R.E. Frosch, and M.R. Yearian, Phys. Rev. **144**, 859 (1966).
- [31] J.C. Bergstrom and E.L. Tomusiak, Nucl. Phys. A **262**, 196 (1976).
- [32] J.C. Bergstrom, U. Deutschmann, and R. Neuhausen, Nucl. Phys. A **327**, 439 (1979).
- [33] F. Eigenbrod, Z. Phys. **228**, 337 (1969).

TABLES

TABLE I. Binding energy,  $B$ , and excitation energy,  $\Delta E$ , of  ${}^6\text{Li}$  states in MeV.

$J^\pi; T$	VMC		GFMC		Expt	
	$B$	$\Delta E$	$B$	$\Delta E$	$B$	$\Delta E$
$2^+; 1$	21.5(1)	5.5(1)	25.5(1)	5.7(1)	26.62	5.37
$2^+; 0$	22.6(1)	4.4(1)	26.8(3)	4.4(4)	27.68	4.31
$0^+; 1$	23.2(1)	3.8(1)	27.3(1)	3.9(1)	28.43	3.56
$3^+; 0$	24.0(1)	3.0(1)	28.5(3)	2.7(3)	29.80	2.19
$1^+; 0$	27.0(1)	—	31.2(1)	—	31.99	—

## FIGURES

FIG. 1. Calculated longitudinal and transverse elastic form factors of the  ${}^6\text{Li}$  ground state are shown in impulse approximation (IA) and with two-body charge and current operators added (IA+MEC) as filled symbols with Monte Carlo statistical error bars. The Coulomb monopole (C0) and quadrupole (C2) contributions to the longitudinal form factor are also shown by the dashed (IA) and solid (IA+MEC) lines. Data are from Refs. [9,28–30].

FIG. 2. Calculated longitudinal and transverse transition form factors to the first four ( $J^\pi; T$ ) excited states of  ${}^6\text{Li}$  are shown in impulse approximation (IA) and with two-body charge and current operators added (IA+MEC). The largest form factor in each case is shown as a point with its statistical error bars; the smaller form factor (if any) is shown by dashed (IA) and solid (IA+MEC) lines. Data are from Refs. [3,4,29,31–33].

Fig.1 Wiringa & Schiavilla

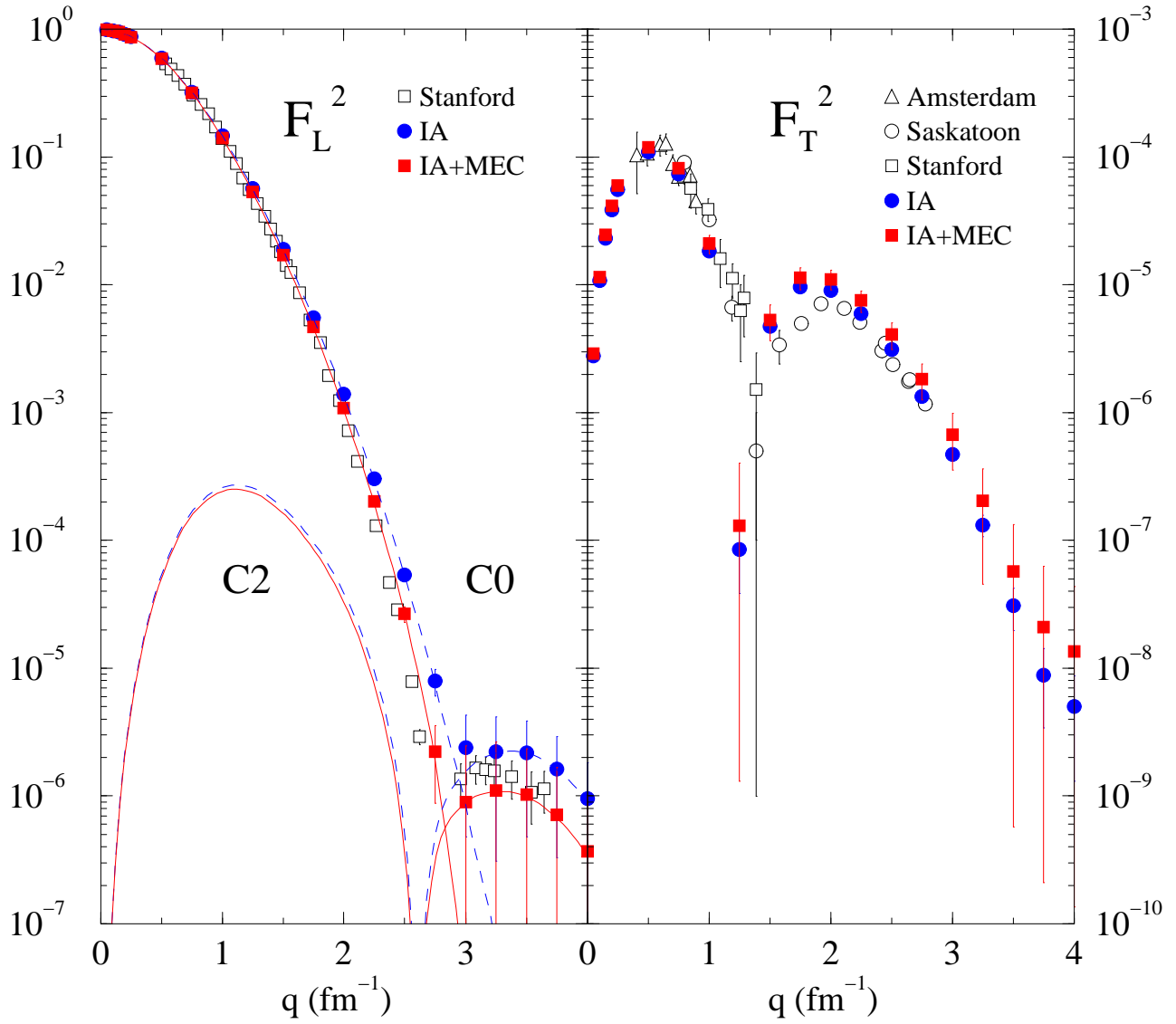


Fig.2 Wiringa & Schiavilla

